Met. Mater. Int., Vol. 16, No. 4 (2010), pp. 553~558
doi: 10.1007/s12540-010-0805-1 Published 26 August 2010

Texture Evolution in FCC Metals from Initially Different Misorientation Distributions under Shear Deformation

H.-J. Chang[1], H. N. Han[1,*], S.-J. Park[2], J.-H. Cho[3], and K. H. Oh[1]

[1]Department of Materials Science and Engineering and Center for Iron & Steel Research, RIAM, Seoul National University, Seoul 151-744, Korea
[2]Korea Institute of Materials Science, 66 Sangnam-dong, Changwon-si, Gyeongnam 641-010, Korea

(received date: 24 September 2009 / accepted date: 7 April 2010)

We applied the crystal plasticity finite element method (CPFEM) based on a rate sensitivity model to examine the subgrain texture evolution of FCC metals under shear deformation. We used two kinds of microstructure models with the same orientation distribution function (ODF) but different spatial arrangements or misorientation distributions (MDs). One contained a great high frequency around low misorientation angles and the other a great high frequency near high misorientation angles. Different misorientation angles among neighboring crystals caused different interactions among them, particularly at the subgrain scale. The difference in MD affected the evolution of texture and average misorientation angles during deformation. The average misorientation angles of the subgrain boundaries increased with shear strain.

Keywords: texture, microstructure, deformation, crystal plasticity, finite element method

1. INTRODUCTION

Extensive experimental work [1,2] and computer simulations [3,4] based on the Taylor model [5] have led to the identification of ideal orientations under shear deformation of FCC polycrystalline materials. These ideal orientations were frequently found under extensive shear deformation. The shear texture components calculated by numerical approaches qualitatively agreed with the experimental results. The intensities of the ideal orientations or shear components predicted under shear deformation, however, had higher values than those of the ideal orientations actually measured. It is known that overestimation of the predicted textures results from using the Taylor assumption of isostrain, or an upper bound solution. Subgrain evolution due to grain interaction between adjacent grains might cause the difference in intensities of texture components. As computational capability and accuracy increase, more detailed microstructure modeling may be considered. Subgrain features and grain boundary characteristics may be modeled using the finite element method and crystal plasticity.

Much research work on subgrain evolution under plastic deformation has been reported based on experimental and numerical approaches [6-9]. Subgrain boundaries were formed by subdivision of grains during plastic deformation, and were controlled by the dislocation glide-induced lattice mismatch in contiguous crystals [7]. Indeed, Nazarov *et al.* [6] modified the polycrystalline model by incorporating a subgrain evolution model, showing that such modification reduced the difference in orientation distribution function (ODF) intensity between numerical calculations and experiments.

In addition to characteristics of the subgrain boundary, those of the grain boundary can play an important role in texturing and microstructure evolution during deformation. Grain boundary characteristics can be expressed by five degrees of freedom, i.e., grain boundary plane normal and misorientation angle/axis. Here, we focused on two-dimensional microstructure modeling, and three degrees of freedom of misorientation angle/axis were mainly used to describe them [10,11]. Misorientation distribution (MD) describes all sets of misorientation angles between adjacent grains in the modeling. The plane normal direction of grain boundaries was set to be a vertical or horizontal line for simplicity. During plastic deformation, inhomogeneities of stress and strain develop as a result of the different crystallographic orientations of adjacent grains. Interactions between grains can be varied by changes in misorientation angle, thus resulting in variations in local stress and strain.

The microstructure construction with subgrains and grain boundary characteristics was a useful approach in order to

*Corresponding author: hnhan@snu.ac.kr

consider inhomogeneity inside grains. It is also effective to arbitrarily construct microstructural features of both ODF and MD for a better understanding of material behavior. The crystal plasticity finite element method (CPFEM) simultaneously satisfies the requirements for strain compatibility and stress equilibrium conditions within an aggregate of grains under an applied load; it is one of the more reliable tools to investigate the heterogeneity of local deformation.

Using a simple two-dimensional microstructure model, we specified initial textures (ODF) and their spatial arrangements or misorientation distributions (MDs) in this study. Two kinds of microstructure models were designed to have the same ODF but a different MD. A single grain consists of nine subgrains, and uniform orientations or random textures were initially specified. The first model has great frequencies at high angle grain boundaries and the second mainly has low angle grain boundaries. The effect of the initial misorientation distribution on the subgrain texture evolution during shearing was examined.

2. SIMULATION PROCEDURE

A commercial code of ABAQUS [12] was used for the FEM simulation. A crystal plasticity model incorporating a rate-dependent slip system constitutive relation described in Peirce *et al.* [13] was implemented in ABAQUS using a user material subroutine, VUMAT. The finite element simulation was carried out based on an arbitrary Lagrangian and Eulerian (ALE) method for large deformations. Details of the crystal plasticity model are reported elsewhere [14-19]. For a rate-dependent material, shear rates are given explicitly in terms of the resolved shear stress on the active slip systems and the resistance of the active slip systems to shear. The rates of shear on the slip systems are expressed according to Peirce *et al.* [13].

$$\dot{\gamma}^{(\alpha)} = \dot{\gamma}_0 \left(\frac{\tau^{(\alpha)}}{g^{(\alpha)}} \right)^{(1/m)} \operatorname{sign}(\tau^{(\alpha)}) \tag{1}$$

where $\tau^{(\alpha)}$ is the shear stress resolved onto the slip plane, $\dot{\gamma}_0$ is a reference shear rate, and m is the strain rate sensitivity. The slip resistance $g^{(\alpha)}$ has an initial value g_0 and evolves with plastic strain on all slip systems according to

$$\dot{g}^{(\alpha)} = \sum_{\beta=1}^{NS} h_{\alpha\beta} \left| \dot{\gamma}^{(\alpha)} \right| \tag{2}$$

The hardening coefficients are

$$h_{\alpha\beta} = h_\beta (q + (1-q)\delta_{\alpha'\beta}) \qquad h_\beta = h_0 \left(1 - \frac{g^{(\beta)}}{g_s} \right)^a \tag{3}$$

where q determines latent-to-self hardening, h_0 is a reference self-hardening coefficient, a is the hardening exponent, and g_s is the slip resistance at which the self and latent hardening coefficients asymptote to zero. The simple shear deformation up to $\gamma = 3$ was calculated and the material properties are listed in Table 1 [17].

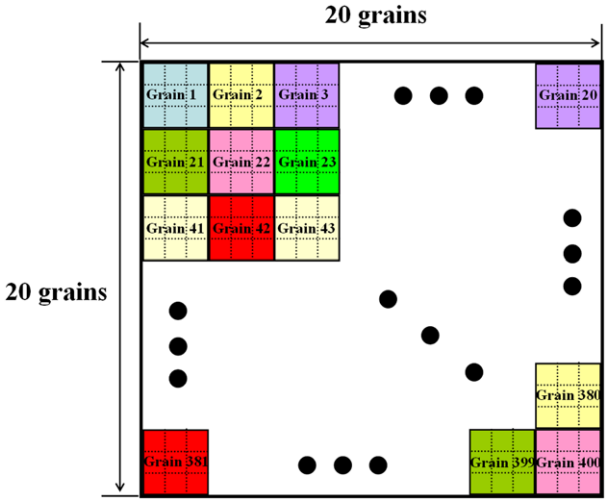

Fig. 1. Microstructure modeling of 400 grains using finite element. Each grain consists of 9 rectangular elements.

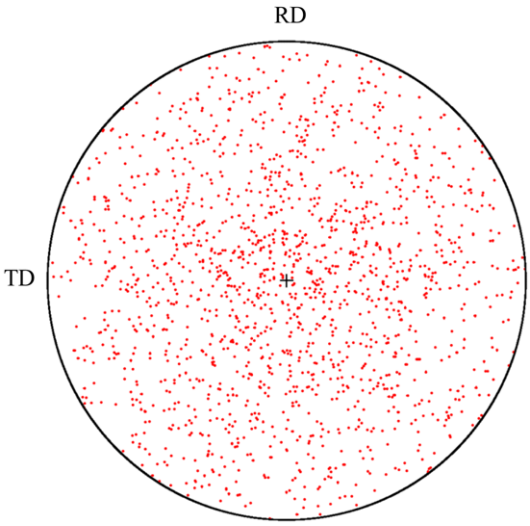

Fig. 2. (111) pole figure for initial 400 grains.

Figure 1 shows a schematic diagram of the initial configuration of microstructure with grains and subgrains. The modeling consisted of 400 grains and each grain contained 9 subgrains. One rectangular element corresponded to a subgrain. The subgrains inside each grain possessed the same initial orientation and could evolve in a different way during deformation. A random distribution with a total of 400 discrete orientations, as shown by the (111) pole figure in Fig. 2, was used for the whole modeling, and a single orientation was given to a single grain, respectively.

In order to obtain various MDs at a given ODF, the optimizing method reported by Miodownik *et al.* [20] was adopted. With this method, the desired MD can be acquired

Table 1. Material parameters for CPFEM [15]

Elastic Moduli	E				n	
	123 GPa				0.34	
Plastic parameters	$\dot{\gamma}_0$	m	a	h_0	g_s	q
	10^{-3}	0.05	2.25	180 MPa	148 MPa	1.0

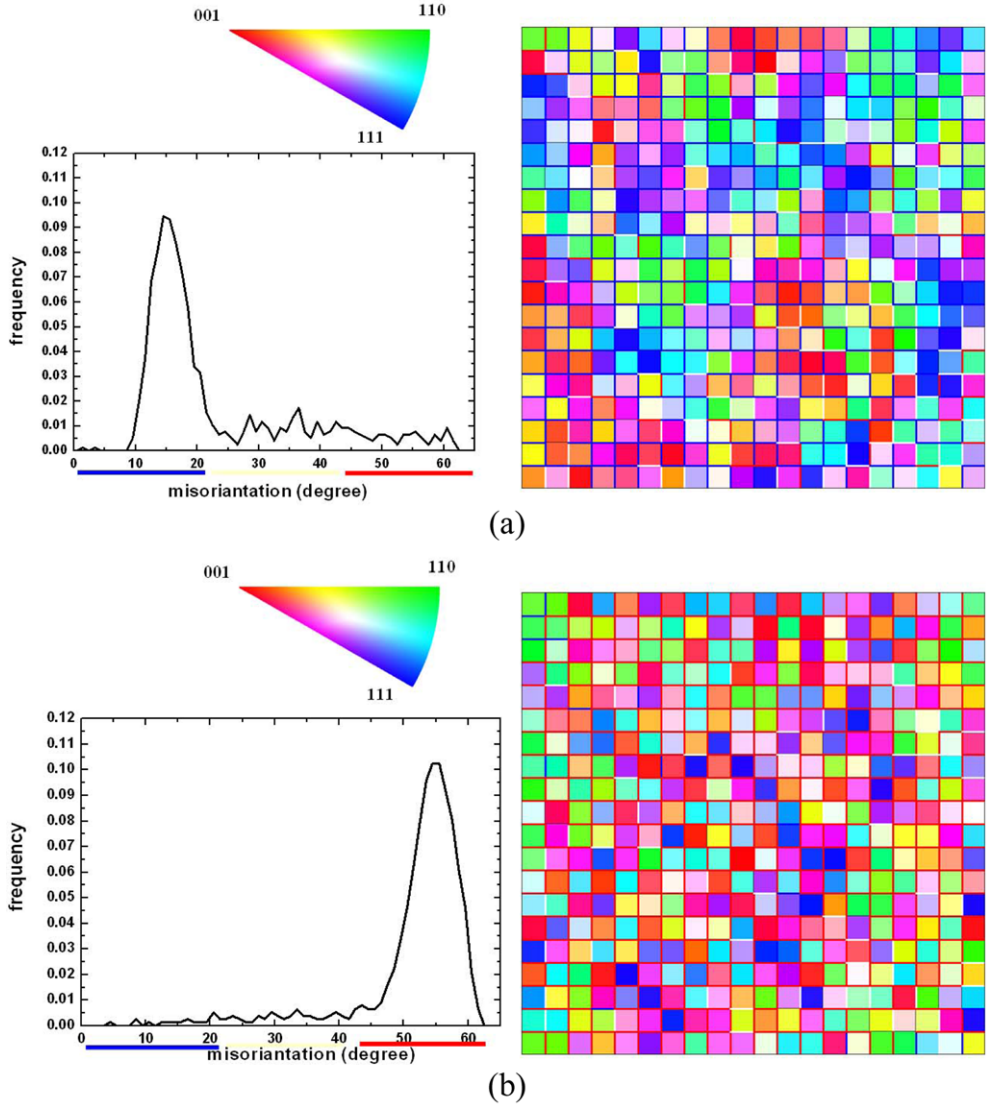

Fig. 3. Initial misorientation angle distributions and FE meshes for (a) L-MD and (b) H-MD. Color index of orientations is also given.

by repeated random switching of selected neighbor orientations only if the switching decreases the difference between a desired MD and an obtained MD. Two different microstructure models were designed in this study, as shown in Figs. 3(a) and (b). The first one named L-MD possessed a low MD and about 90 % of the frequency was located between 10° and 20° (Fig. 3(a)). The red, green and blue colors inside the grains represent the (001), (110) and (111) orientations, respectively. Note the triangle map for orientation color codes. The blue, white and red lines at the grain boundaries indicate the low (1° to 20°), middle (21° to 40°) and high (41° to 60°) misorientation angles, respectively. The second models called H-MD mainly contained high angle misorientations and about 90 % of the frequency was placed between 50° and 60° (Fig. 3(b)). In cubic metals, the maximum misorientation angle is given as 62.8° [21].

3. RESULTS AND DISCUSSION

Texture evolution from initial random orientations of

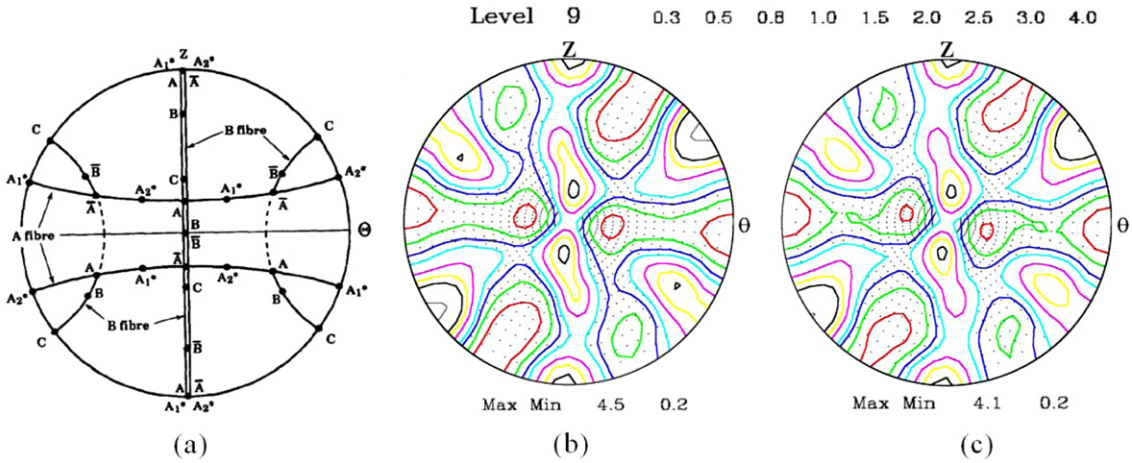

Fig. 4. (111) pole figures after shear strain of $\gamma = 3$: (a) ideal orientations pertaining to fiber textures [4], (b) prediction for the L-MD and (c) prediction for the H-MD.

cubic materials was observed during simple shear deformation. Ideal orientations found during simple shear are usually represented by two fibers, which are referred to as A: {111}<uvw> and B: {hkl}<110> in Fig. 4(a) [4]. The vectors {hkl} and <uvw> were aligned with the shear plane normal (Z) and the direction of the applied shear (θ), respectively. Figures 4 (b) and (c) depict the (111) pole figures after shear deformation, $\gamma = 3$ for microstructure with L-MD and H-MD cases, respectively. Overall, calculated (111) pole figures for both L-MD and H-MD were similar to the typical shear texture, as shown in Fig. 4(a). Some differences in intensity existed between L-MD and H-MD. The pole figure of the L-MD case had a higher intensity than that of the H-MD. Orientations located along the B fiber, particularly C components, mainly displayed increased intensity. On the other hand, orientations along the A fiber displayed intensities similar to each microstructure modeling. Although the initial misorientation distribution did not greatly affect overall trends of shear texture evolution, the initial low misorientation angle appeared to give a slightly higher intensity along the B fiber than along the A fiber.

Figures 5(a) and (b) show shear stress distributions after a shear strain of $\gamma = 3$ for two different microstructures. Microstructure with the L-MD (Fig. 5(a)) initially had great high frequencies near low angle grain boundaries, and thus a bundle of surrounding grains could have low angle grain boundaries. These bundles can act as virtually extended grains under shearing. In Fig. 5(a), broad regions more than a single grain displayed similar stress levels and looked like a large deformed grain. The broad regions in the microstructure with the L-MD had orientations near the B fiber, and easily accepted shear deformation. Those "soft" orientations accommodated a comparatively great amount of deformation during shearing. This resulted in the high intensity of B fiber in the L-MD microstructure. Microstructure with the H-MD

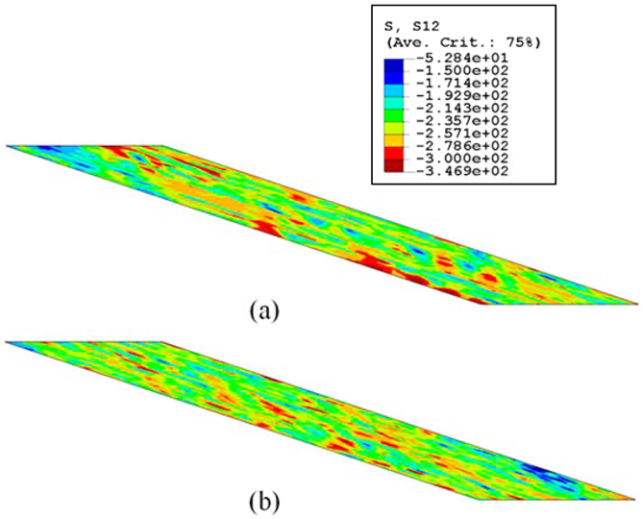

Fig. 5. Shear stress distributions after shear strain of $\gamma = 3$ obtained from FEM simulations with the (a) L-MD and (b) H-MD.

(Fig. 5(b)), however, had more local variation in shear stress than that with the L-MD. This means that the interaction between neighboring grains in the microstructure with the H-MD was more severe than that observed between neighboring grains with the L-MD.

Figure 6 presents changes of misorientation angle distribution with shear strain. Although both microstructures with the L-MD and the H-MD had few frequencies less than 10° as shown in Figs. 3(a) and (b), the highest peaks were found in misorientation angles less than 10° during shear deformation. This is because orientations of subgrains inside grains evolved during shearing. Since the misorientation angles between subgrains increased with deformation [9], the height and shape of the peaks in the low angle distributions gradually decreased and grew broader, respectively. Some differ-

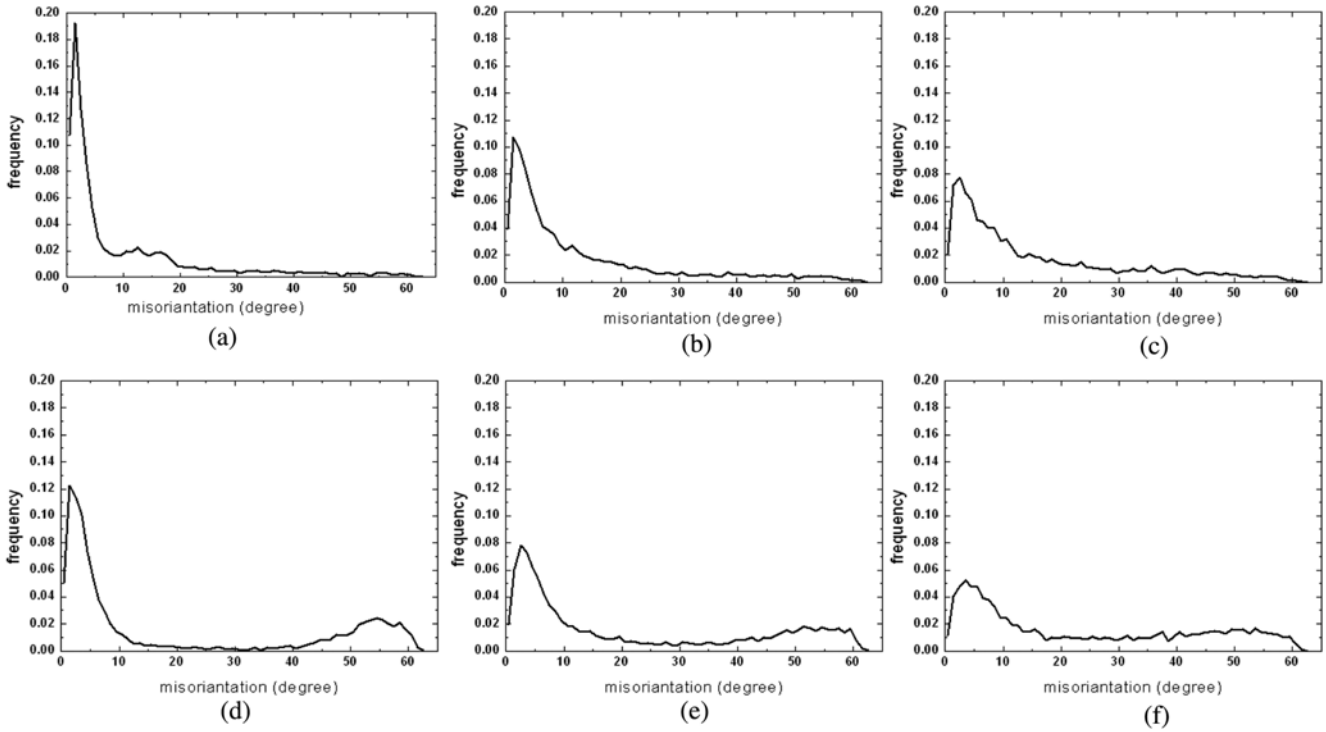

Fig. 6. Evolution of misorientation distributions from L-MD or H-MD during shearing. (a) L-MD at $\gamma = 1$, (b) L-MD at $\gamma = 2$, (c) L-MD at $\gamma = 3$, (d) H-MD at $\gamma = 1$, (e) H-MD at $\gamma = 2$ and (f) H-MD at $\gamma = 3$.

ence existed in the decreasing rate of the peak height and the broadening rate of the peak shape between the L-MD and the H-MD. In particular, the broadening rate of the peak shape for the H-MD was faster than that for the L-MD.

Figure 7 shows variations of average misorientation angles in the subgrain boundaries with Mises strain. The average values for both microstructures with the H-MD and the L-MD increased with shear strain. Subgrains or subdivisions found inside a grain were due to inhomogeneous deformation caused by an outbound interaction [7]. High angle boundaries can easily produce inhomogeneous deformation inside grains, because neighboring grains have different slip systems activated during deformation. At the same time, low angle boundaries certify similar slip systems activating between neighboring grains. This means that two grains with a low misorientation angle have a weak interaction between each other. And thus the subgrain evolution should be more active in the microstructure with the H-MD than in the microstructure with the L-MD. The increase in average misorientation angle also should be higher in the H-MD than in the L-MD. Figures 6 and 7 indicate that subgrain evolution is strongly related with initial misorientation distributions.

Note that the slopes of average misorientation angles in Fig. 7 look similar to both microstructures with the H-MD and the L-MD. Both slopes of the average misorientation angles are about 1.0. The slope calculated here is higher than the value experimentally determined by Hughes *et al.* [9],

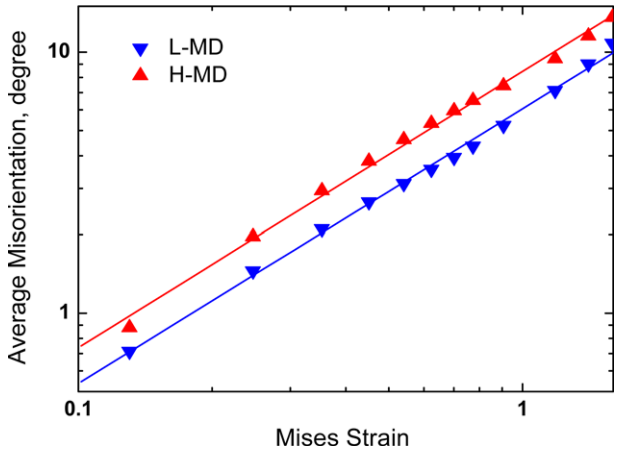

Fig. 7. Average misorientation angle with Mises strain for the L-MD and H-MD.

which was approximately 0.67. Several studies calculated by FEM simulation have reported that the slope was around 1.0 [6,22,23], similar to our results. The slope overestimated by FEM approaches may have originated from various causes. Subgrain evolution was implied to be one of the reasons as pointed out before. Although we computed texture and microstructure evolution with the simplified modeling, and major microstructural features during deformation were captured well, the limited number of subgrains or discretization still affected computational accuracy. To better understand

the microstructure evolution, more discretization of subgrains and three-dimensional approaches still need to be adopted.

4. SUMMARY

The two-dimensional crystal plasticity finite element method was applied to examine the subgrain texture evolution of FCC metals under shear deformation. Two kinds of microstructure modeling with the same ODF but different MDs were used. Microstructures with different MDs affected the evolution of texture and the average misorientation angles. In a microstructure with a great high frequency at low angle grain boundaries, a bundle of adjacent grains deformed together. A microstructure with a great frequency at high angle grain boundaries had localized deformation due to severe interaction between neighboring grains. The average misorientation angles of subgrain boundaries increased with applied shear strain. The slope of the average misorientation angles predicted were overestimated compared with experiments. Finer mesh discretization for subgrains and three-dimensional approaches would be helpful to better understand microstrucural evolution.

ACKNOWLEDGMENTS

This work was supported by a National Research Foundation of Korea grant funded by the Ministry of Education, Science and Technology (2009-0083038). K.H. Oh received support from a Korea Science and Engineering Foundation (KOSEF) grant provided by the Korean government (MOST) (No.R11-2005-065).

REFERENCES

1. W. A. Backofen, *Trans. AIME.* **188**, 1454 (1950).
2. F. Montheillet, M. Cohen, and J. J. Jonas, *Acta metall.* **32**, 2077 (1984).
3. J. G. Sevillano, P. V. Houtte, and E. Aernoudt, *Z. Metallk.* **66**, 367 (1975).
4. L. S. Toth, P. Gilormini, and J. J. Jonas, *Acta metal.* **36**, 3077 (1988).
5. G. I. Taylor, *J. Inst. Metals* **62**, 307 (1938).
6. A. A. Nazarov, N. A. Enikeev, A. E. Romanov, T. S. Orlova, I. V. Alexandrov, I. J. eyerlein, and R. Z. Valiev, *Acta mater.* **54**, 985 (2006).
7. N. Hansen, *Scripta metall. mater.* **27**, 1447 (1992).
8. D. Kuhlmann-Wilsdorf and N. Hansen, *Scripta metall. mater.* **25**, 1557 (1991).
9. D. A. Hughes, Q. Liu, D.C. Chrzan, and N. Hansen, *Acta mater.* **45**, 105 (1997).
10. J.-H. Cho, *Adv. Mat. Res.* **26-28**, 1003 (2007).
11. V. Rnadle, *The Measurement of Grain boundary Geometry*, Institute of Physics Publishing (1993).
12. ABAQUS version 6.5, *Analysis User's manual*, Hibbitt, Karlsson and Sorensen, Pawtucket, RI (2004).
13. D. Peirce, R. J. Asaro, and A. Needleman, *Acta metall.* **31**, 1951 (1983).
14. R. J. Asaro and A. Needleman, *Acta metall.* **33**, 923 (1985).
15. S. R. Kalidindi, C. A. Bronkhorst, and L. Anand, *J. Mech. Phys. Solids* **40**, 537 (1992).
16. S.-J. Park, S.-H. Choi, K. H. Oh, and J. A. Szpunar, *Mater. Sci. Forum* **408-412**, 377 (2002).
17. S.-J. Park, *Ph.D. thesis*, Seoul National Univ., Seoul, Korea (2000).
18. Y.-S. Song, B.-J. Kim, H.-W. Kim, S.-B. Kang, and S.-H. Choi, *J. Kor. Inst. Met. & Mater.* **46**, 135 (2008).
19. Y.-S. Song, D.-W. Kim, H.-S. Yang, S.-H. Han, K.-G. Chin, and S.-H. Choi, *J. Kor. Inst. Met. & Mater.* **47**, 274 (2009).
20. M. Miodownik, A. W. Godfrey, E. A. Holm, and D. A. Hughes, *Acta mater.* **47**, 2661 (1999).
21. J. K. Mackenzie, *Biometrika* **45**, 229 (1958).
22. P. R. Dawson, D. P. Mika, and N. R. Barton, *Scripta mater.* **47**, 713 (2002).
23. D. P. Mika and P. R. Dawson, *Acta. mater.* **47**, 1335 (1999).